

# Spectroscopic Diagnostics for Spatial Density Distribution of Plasmoid by Pellet Injection in the Large Helical Device

Gen MOTOJIMA, Ryuichi SAKAMOTO, Motoshi GOTO, Hiroshi YAMADA and  
LHD experiment group

*National Institute for Fusion Science, 322-6 Oroshi-cho, Toki 509-5292, Japan*

(Received 1 February 2009 / Accepted 21 June 2009)

To investigate the behavior of a plasmoid consisting of pellet ablatant ionized by background plasma, two dimensional imaging measurements of high-speed spectroscopy have been developed using a fast camera in the Large Helical Device (LHD). The diagnostic system provides density distribution of the plasmoid. The density distribution is determined using the Stark broadening width of the Balmer- $\beta$  line. Stark broadening profile can be evaluated from the intensity ratio measured using narrow-band optical filters having different full width at half maximum. Two dimensional images of the plasmoid are obtained by a fast camera connected to a bifurcated fiber scope with two objective lenses. An initial result shows that the plasmoid density is obtained within a factor of 2 by imaging measurements.

© 2010 The Japan Society of Plasma Science and Nuclear Fusion Research

Keywords: pellet injection, plasmoid, imaging measurement, spectroscopy, LHD, helical device

DOI: 10.1585/pfr.5.S1033

## 1. Introduction

Solid hydrogen pellet injection is a primary technique used for efficient core plasma fueling in fusion devices. Pellet injection surely plays an important role in next-step devices such as ITER and it will also be a promising candidate in a future fusion reactor for particle refueling. In particular, the importance of pellet injection is accentuated in the high central density operation required for a helical reactor [1].

When pellets are injected in a hot and magnetically confined background plasma, pellet particles are ablated with heat flux from the background plasma. The pellet is immediately surrounded by the neutral cloud generated by its ablation. The neutral cloud shields the pellet particles from the ambient background plasma. As a result, the neutral cloud is ionized and expanded in a direction parallel to the magnetic field lines. Here, the ionized pellet material is referred to as a plasmoid.

Pellet ablation and subsequent behavior of the plasmoid are key elements in determining the characteristics of pellet fueling. Extensive experiments have been performed with the objective of clarifying fueling characteristics of the pellet [2]. In particular, recent studies have focused on the drift of the plasmoid [3]. The drift of the plasmoid could be attributed to an  $\mathbf{E} \times \mathbf{B}$  drift that is caused by vertical polarization in the ablation cloud due to magnetic field gradient [4]. The behavior of the plasmoid following the ablation process has a primary effect on the pellet mass deposition. Therefore, understanding not only pellet ablation but also the subsequent behavior of the plasmoid

helps in optimizing pellet fueling. As for the understanding of pellet ablation, the identification of position of the pellet ablation is of great importance. In the LHD, a three dimensional observation system for stereoscopic analysis has been developed using a fast camera [5]. The position of pellet ablation can be identified precisely by this method. Concerning the understanding of plasmoid behavior, the quantitative evaluation of the pellet particles transferred by the plasmoid is of great importance. This homogenization process has been demonstrated in numerical calculations. Moreover, the density and temperature of the plasmoid have been measured by spectroscopic diagnostics [6, 7]. However, a quantitative two dimensional evaluation of plasmoid parameters has not yet been achieved. The objective of this study is to evaluate quantitatively the two dimensional density distribution in the plasmoid on the basis of imaging measurements with high-speed spectroscopic diagnostics.

The rest of the paper is organized as follows. The principle of high-speed spectroscopic analysis is described in Section 2. In Section 3, the experimental setup is presented. The initial experimental results are described in Section 4, and a summary is provided in Section 5.

## 2. Imaging Measurements of High-speed Spectroscopy

The spectra of Balmer-lines and continuum are determined by the density and temperature of the plasmoid. Here, the emission from the background plasma can be ignored, because the density of the plasmoid is several hundred times greater than that of the background plasma.

author's e-mail: [motojima.gen@lhd.nifs.ac.jp](mailto:motojima.gen@lhd.nifs.ac.jp)

The electron density can be determined from the Stark broadening profile of the Balmer-lines. In this study, it is noted that the spectra are estimated from the fitting with the theoretical data. In the theoretical data, the intensity of the spectra is calculated on the assumption of local thermodynamic equilibrium [7]. The broadening profile of the spectra is calculated using Ref. [8].

Figure 1 shows examples of spectra around the Balmer- $\beta$  line (center wavelength: 486.1 nm) in a wavelength range 470-500 nm for (a) low density ( $n_e = 1.0 \times 10^{22} \text{ m}^{-3}$ ) and (b) high density ( $n_e = 1.0 \times 10^{23} \text{ m}^{-3}$ ). The same electron temperature of 1.0 eV is assumed for both cases (the value is based on the results from Ref. [7]). In the low density case, the line profile exhibits a peak, whereas in the high density case, the line profile is broader. It is found that the line profile depends on the electron density. The characteristics enable an evaluation of the electron density.

Stark broadening width can be estimated from the intensity ratio measured using narrow-band optical filters having different full width at half maximum (FWHM). The ratio of intensity with narrow bandwidth to that with wide

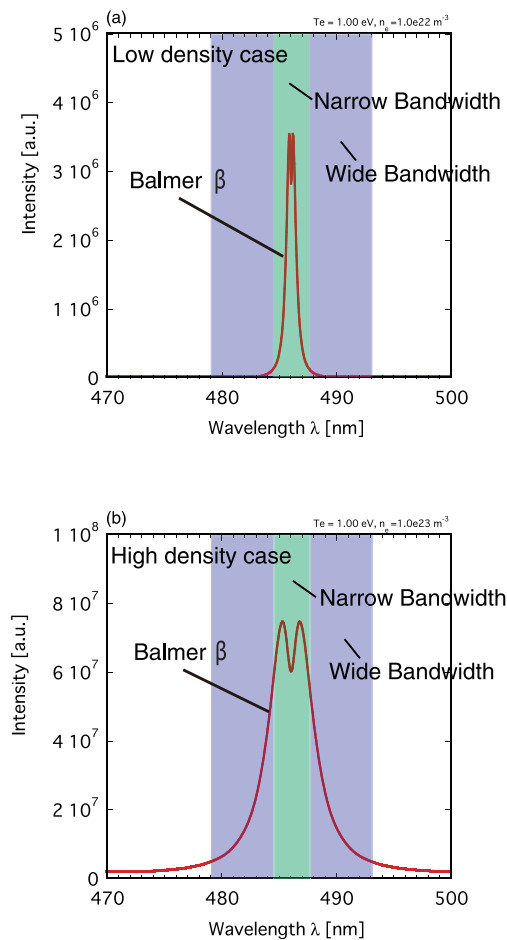


Fig. 1 Spectra of the Balmer- $\beta$  with a constant background for (a) low density ( $n_e = 1.0 \times 10^{22} \text{ m}^{-3}$ ) and (b) high density ( $n_e = 1.0 \times 10^{23} \text{ m}^{-3}$ ). Intensity is expressed on a linear scale.

bandwidth is expressed as

$$\frac{I_{\text{narrow}}}{I_{\text{wide}}} = \frac{\int I(\lambda) \times T_{\text{narrow}}(\lambda) d\lambda}{\int I(\lambda) \times T_{\text{wide}}(\lambda) d\lambda}, \quad (1)$$

where  $I_{\text{narrow}}$  and  $I_{\text{wide}}$  are the intensity with narrow bandwidth and that with wide bandwidth, respectively, and  $I$  is the intensity of the spectrum.  $\lambda$  is the wavelength, and  $T_{\text{narrow}}$  and  $T_{\text{wide}}$  are the transmission rates with narrow bandwidth and with wide bandwidth, respectively. In the low density case, there is almost no difference in the intensity between wide and narrow bandwidths due to the peaked line profile, indicating that intensity ratio defined as intensity with narrow bandwidth to that with wide bandwidth approaches unity. In the high density case, the intensity difference becomes large due to a broader line profile, resulting that the ratio becomes smaller than unity.

In this study, we concentrate on the Balmer- $\beta$  line to evaluate the density of the plasmoid, because the influence of the self-absorption effect on the Balmer- $\beta$  line profile is negligible while the Balmer- $\alpha$  line profile is affected by it [7] and the Balmer- $\gamma$  line intensity is much small. The filter parameters suitable for various presumed densities ( $10^{22}$ - $10^{24} \text{ m}^{-3}$ ) and temperatures (0.9-1.2 eV) in a plasmoid are selected on the basis of the spectra estimated from the theoretical data. The density and temperature ranges are assumed based on results obtained from spectrometer measurements of plasmoids in LHD [7]. The filter combination of same central wavelength of 486.1 nm and different FWHM of 5 nm and 20 nm prove the dependence on electron density very clearly independent of the electron temperature. Figure 2 shows dependence of the logarithm of electron density on the ratio of the intensity with FWHM of 5 nm to that with a wider FWHM of 20 nm. Using this filter combination, the ratio becomes approximately pro-

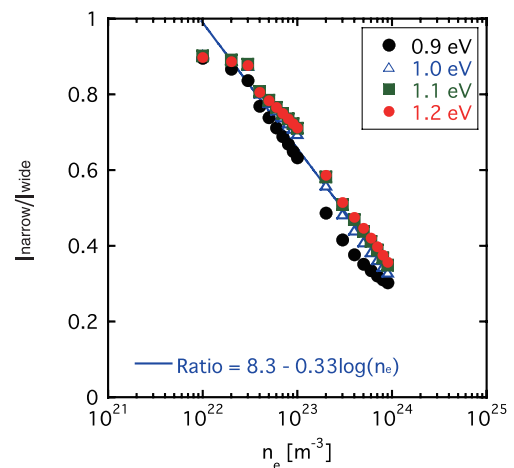


Fig. 2 Dependence of the logarithm of density on the ratio of the intensity measured with FWHM of 5 nm to that measured with a wide FWHM of 20 nm. Solid line shows logarithmic fitting of the data. The fitting line is used in analysis.

portional to the logarithm of plasmoid density by a factor of about 2 under the assumption that the temperature is in the range from 0.9 to 1.2 eV. The ratio becomes smaller with increasing electron density. With this filter combination, we can measure the plasmoid density in the range from  $10^{22}$  to  $10^{24} \text{ m}^{-3}$ .

### 3. Experimental Setup

In this section, the spectroscopic diagnostics system for measuring the density distribution of a plasmoid is explained. Figure 3 (a) shows a horizontally elongated poloidal cross section of the LHD and an in-situ pipe gun type 10 barrel pellet injector. The nominal pellet size is  $3.4 \text{ mm } \phi \times 3.4 \text{ mm } l$ . The typical pellet speed is 1000 m/s. Doppler shift can be neglected because the shift is only  $10^{-3} \text{ nm}$  at 486.1 nm. The plasmoid can be observed just behind the pipe gun pellet injector and parallel to the injection axis. In other words, the line of sight coincides with the pellet injection axis. The emission from the plasmoid is evenly divided with a half mirror, as shown in Fig. 3 (b).

A bifurcated fiber scope with two objective lenses is used in this spectroscopic system [5]. The scope is composed of a pair of 50000 element quartz fiber scopes having a flexible protective tube made of stainless-steel. The overall length is 15 m, and the bifurcated portions are about 5 m in length. Each objective lens, which has a field of view of 15 degrees, is used with the filters selected as described in Section 2. Wavelength characteristics of filters are not important in this study because the field of view in the observed area of plasmoid is about 2 degrees which lead to blue shift of about 0.4 nm at 486.1 nm. The optical filters are calibrated using a standard light source. Two images viewed from the same line of sight located just behind the pellet injector are obtained. The images are focused onto a

single fast camera (Vision Research Inc., Phantom V7) so that simultaneity is ensured. The observation of a identical location is ensured by comparing the strength between the two images. The fast camera is equipped with a 12-bit self-resetting complementary metal oxide semiconductor (SR-CMOS) sensor. The selected frame rate and exposure time with a resolution of  $464 \times 192$  pixels are 20000 fps and  $2 \mu\text{s}$ , respectively. One pixel corresponds to 4–5  $\mu\text{m}$ , which is enough to reveal the density distribution in the plasmoid of several dozen cm in size. The pellet moves 2 mm during the exposure time. However, the movement is within 1 pixel, which does not affect the measurement. As shown in Fig. 3 (c), the bundled end is connected to an imaging lens that projects a pair of images onto the imaging sensor.

### 4. Results

Initial results of two dimensional imaging measurements conducted by high-speed spectroscopy were obtained. Figure 4 shows typical images of the plasmoid with the filters having (a) FWHM 5 nm and (b) FWHM 20 nm. Nonuniformity on the background is caused by the characteristics of the high speed camera. The pellet is injected into the NBI plasma with a central electron temperature of 1.5 keV. The intensity of the image obtained using a filter of FWHM 20 nm is stronger than that of the image obtained using a filter of FWHM 5 nm. It seems that the plasmoid expands in a direction parallel to the magnetic field line. Fig. 5 (a) shows the emission intensity distribution of two images in a direction perpendicular to the magnetic field line passing through the maximum intensity point. An intensity difference is observed in the pellet ablatant.

Figure 5 (b) shows the intensity ratio of the two images in a direction perpendicular to the magnetic field line

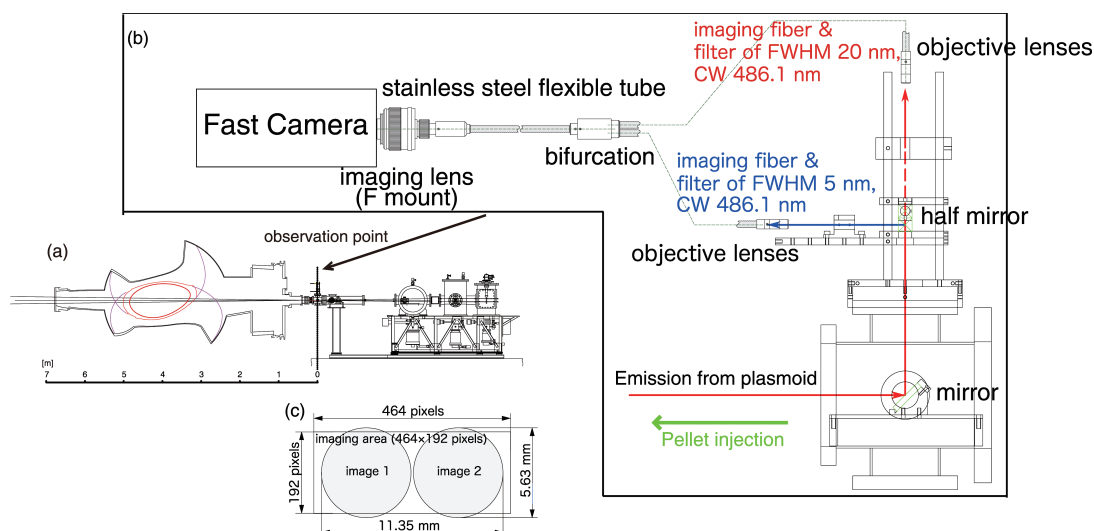


Fig. 3 (a) Cross-sectional drawing of the LHD vacuum vessel and fuelling pellet injector, which is equipped with 10 independent barrels, (b) enlarged view of observation point where the imaging measurements are performed, (c) imaging area of the sensor of the fast camera.

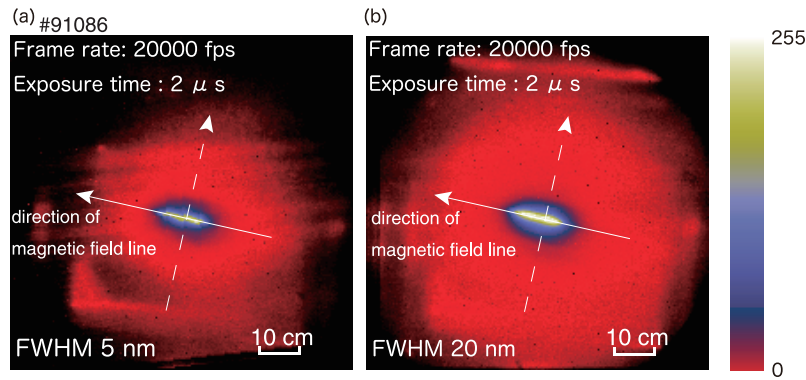


Fig. 4 Typical images of a plasmoid with the filters having (a) FWHM of 5 nm and (b) FWHM of 20 nm. Solid line shows the direction of the magnetic field line; dashed line shows the direction perpendicular to the magnetic field line.

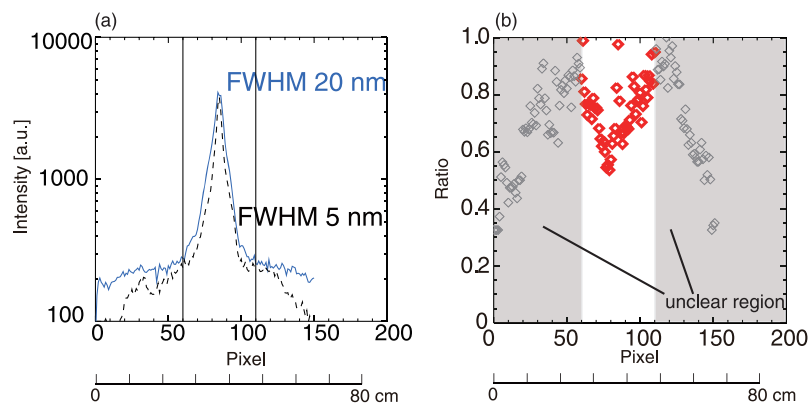


Fig. 5 (a) Emission intensity distribution and (b) ratio of two images in a direction perpendicular to the magnetic field line passing through the maximum intensity point. Solid line represents the intensity with a FWHM of 20 nm, and dashed line represents the intensity with FWHM of 5 nm.

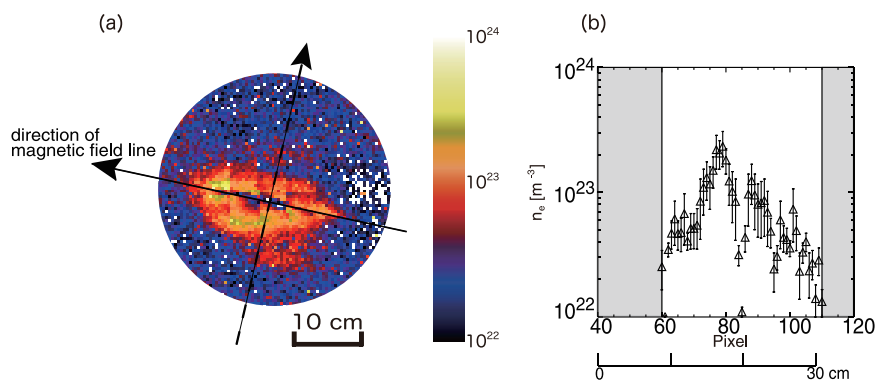


Fig. 6 (a) Density distribution in the plasmoid and (b) electron density distribution along the dashed line in a direction perpendicular to the magnetic field line passing through the maximum intensity point. Here, solid line shows the direction of the magnetic field line; dashed line shows the direction perpendicular to the magnetic field line.

passing through the maximum intensity point. In the region around the center of the plasmoid, the minimum of the intensity ratio is about 0.5, which indicates a density of the order of  $10^{23} \text{ m}^{-3}$ . The ratio tends to unity with increasing distance from the center of the plasmoid, indicating a density of the order of  $10^{22} \text{ m}^{-3}$ . The center of plasmoid

is defined as the strongest intensity point of the emission. The emission observed at each pixel is assumed to have a representative density at each point. In future, the line-of-sight integration effect will be taken into account.

In this study, the analysis is limited to the region around the plasmoid, because it might be difficult to eval-

uate the intensity ratio in the outer region of the plasmoid due to a temperature higher than that assumed due to the effect of the background plasma. However, it should be noted that the ratio in the unclear region seems to change monotonically. This might be due to the increment of intensity of the continuum caused by higher temperature. Therefore, further analysis is required.

Figure 6 (a) shows the density distribution in the plasmoid. The plasmoid has dimensions such that its width of roughly 10 cm is oriented perpendicular to the magnetic field line and its length of 20 cm is oriented parallel to the magnetic field line. The size of plasmoid is defined as the area with significant intensity of the emission. Plasmoid density is of the order of  $10^{23} \text{ m}^{-3}$  except in the center region of the plasmoid. In the center region of the plasmoid, it seems that the density is lower. The reason might be attributed to the actual temperature range being lower than that assumed. However, further studies are necessary. Figure 6 (b) shows the electron density distribution in a direction perpendicular to the magnetic field line passing through the maximum intensity point. A maximum electron density of  $2.3 \pm 0.7 \times 10^{23} \text{ m}^{-3}$  is observed.

## 5. Summary

To obtain the two dimensional plasmoid density distribution quantitatively, imaging measurements of a high-speed spectroscopic system using a fast camera have been developed. The density of the plasmoid is evaluated using the width of Stark broadening in the Balmer- $\beta$  line. Stark broadening can be estimated comparing the difference in emission intensity from the plasmoid obtained using narrow-band optical filters having different bandwidth. The most suitable pair of filters, which have the same central wavelength of 486.1 nm and different FWHM of 5 nm

and 20 nm, respectively, was selected on the basis of spectra estimated from the fitting with the theoretical data. As an initial result, the density distribution of the plasmoid was obtained within a factor of 2 by imaging measurements. Here, we show that the plasmoid density is of the order of  $10^{23} \text{ m}^{-3}$ . The plasmoid has a 10 cm width perpendicular to the magnetic field line and 20 cm length parallel to the magnetic field line. In future, the temperature distribution of the plasmoid will be measured comparing the intensity of the Balmer- $\beta$  line and the continuum. Furthermore, the three dimensional distribution of the plasmoid density will be evaluated using tomography base on the assumption that the structure of the plasmoid is rotational axial-symmetry around the magnetic field line.

## Acknowledgements

The authors would like to thank the LHD operation group. They are also grateful to Professor O. Motojima (General director of NIFS) for his continuous encouragement. This study was supported by NIFS08ULPP521.

- [1] O. Mitarai *et al.*, Proc. 22nd IAEA Fusion Energy Conference, Geneva, FT/P3-19 (2008); also available at [http://www-pub.iaea.org/MTCD/Meetings/FEC2008/ft\\_p3-19.pdf](http://www-pub.iaea.org/MTCD/Meetings/FEC2008/ft_p3-19.pdf)
- [2] B. Pégourié, Plasma Phys. Control. Fusion **49**, R87 (2007).
- [3] P. T. Lang *et al.*, Phys. Rev. Lett. **79**, 1487 (1997).
- [4] V. Rozhansky *et al.*, Plasma Phys. Control. Fusion **37**, 399 (1995).
- [5] R. Sakamoto *et al.*, Rev. Scient. Inst. **76**, 103502 (2005).
- [6] D. H. McNeill *et al.*, Phys. Fluids B **3**, 1994 (1991).
- [7] M. Goto *et al.*, Plasma Phys. Control. Fusion **49**, 1163 (2007).
- [8] C. Stehle and R. Hutcheon, Astron. Astrophys. Suppl. Ser. **140**, 93 (1999).